Research Square

Preprints are preliminary reports that have not undergone peer review.
They should not be considered conclusive, used to inform clinical practice,
or referenced by the media as validated information.

In-season Patterns and Environmental Drivers of Aflatoxin Contamination Across Peanut Seed Size Fractions

Sara Maktabi

Sara.Maktabi@uga.edu

University of Georgia

Leonardo Mendes Bastos

University of Georgia

Cristiane Pilon

University of Georgia

George Vellidis

University of Georgia

Research Article

Keywords: drought stress, environmental drivers, spline regression, machine learning, TreeSHAP, spatial heterogeneity

Posted Date: November 11th, 2026

DOI: https://doi.org/10.21203/rs.3.rs-11449573/v1

License: This work is licensed under a Creative Commons Attribution 4.0 International License.
Read Full License

Additional Declarations: No competing interests reported.

In-season Patterns and Environmental Drivers of Aflatoxin Contamination Across Peanut Seed Size Fractions

Sara Maktabi[1,2], Leonardo Mendes Bastos[2,3], Cristiane Pilon[1,2], George Vellidis[1,2]

[1] Department of Crop & Soil Sciences, University of Georgia, Tifton, GA
[2] Institute for Integrative Precision Agriculture, University of Georgia, Athens, GA
[3] Department of Crop & Soil Sciences, University of Georgia, Athens, GA
Corresponding author: Sara Maktabi, Sara.Maktabi@uga.edu

Abstract

Aflatoxin contamination in peanut is highly variable across the growing season and may differ among seed fractions and locations within a field. Understanding its temporal dynamics, environmental associations, and spatial heterogeneity is essential for developing targeted aflatoxin risk-assessment and management strategies. This study aimed to characterize temporal, environmental, and spatial patterns of aflatoxin contamination in larger and smaller peanut seed fractions across commercial rainfed fields in Georgia and to evaluate the ability of environmental variables to predict contamination and deviations from expected seasonal patterns. Repeated in-season sampling was conducted in five commercial rainfed peanut fields. Sampling time was standardized using days after planting (DAP). Statistical inference, nonlinear seasonal modeling, and machine-learning analyses were integrated to evaluate seed-fraction differences, characterize seasonal contamination trajectories, and identify environmental predictors. Model performance was assessed using nested cross-validation with inner-fold hyperparameter optimization, permutation importance, TreeSHAP analysis, and leave-one-field-out validation. Spatial visualization was used to characterize within-field contamination heterogeneity across sampling events. Seed-fraction differences were seasonally dependent, with significantly greater contamination in the smaller fraction during middle sampling events but no significant differences at the beginning or end of the sampling period. Environmental prediction was stronger for direct contamination than for deviations from expected in-season trajectories. The best models explained 27.1% and 41.6% of direct-contamination variability in the larger and smaller fractions, respectively, compared with 10.9% and 18.6% of in-season-deviation variability. Permutation importance and TreeSHAP analyses consistently identified short-term moisture and thermal conditions, particularly recent rainfall, dry-day accumulation, and temperature metrics, as important predictive signals, although their relative contributions differed between seed fractions and prediction targets. Spatial visualization revealed substantial within-field heterogeneity across sampling events. Predictive performance declined when entire fields were withheld, indicating limited transferability to previously unseen fields. Overall, aflatoxin contamination exhibited temporally dynamic, spatially heterogeneous, and seed-fraction-specific patterns associated with short-term environmental conditions. These findings provide a framework for identifying periods and locations of elevated aflatoxin contamination risk and support the development of field-specific, temporally informed risk-assessment approaches. The limited transferability across fields highlights the need for broader multi-field validation before applying predictive models to new production environments or precision management decisions.

Keywords: drought stress; environmental drivers; spline regression; machine learning; TreeSHAP; spatial heterogeneity

1. Introduction

Peanut (*Arachis hypogaea* L.) is an economically important crop widely grown for food, oil, and other products. Peanuts are the most consumed nut worldwide and the state of Georgia produces

more than half of the peanut grown in the United States (USDA-NASS). Because peanut kernels develop underground, their quality and marketability can be strongly influenced by environmental conditions in the pod zone, particularly temperature and soil moisture, as well as insect and fungal activity during the late stages of kernel development (Hill et al., 1983; Cole et al., 1985; Bowen and Hagan, 2015; Danso et al., 2024). These environmental conditions can favor the growth of aflatoxigenic fungi, particularly *Aspergillus flavus*, and promote aflatoxin production in developing peanut kernels.

Aflatoxin is one of the most potent naturally occurring mycotoxins, and its presence in peanuts and peanut products is of particular concern given the link between chronic exposure and hepatocellular carcinoma and other health effects (Koshiol et al., 2026). Because of these risks, maximum allowable aflatoxin levels for peanuts intended for direct human consumption are very low, for example, 2 µg/kg for aflatoxin B1 and 4 µg/kg for total aflatoxins in the European Union (EU), with somewhat higher but still stringent limits for lots destined for sorting or further processing (EU, 2010). Hereafter, aflatoxin concentrations are expressed in parts per billion (ppb), where 1 ppb is equivalent to 1 µg/kg. Comparable thresholds apply in the U.S. and international trade systems, where contaminated shipments can be rejected or diverted to lower-value markets (US FDA, 2025). These regulations leave a very small margin of error for commercial peanut production systems.

Preharvest aflatoxin contamination is generally sporadic and patchy. Many fields or sampling locations show levels near the non-detectable limit, while others show high, difficult-to-predict levels, particularly when contamination is unevenly distributed among kernel fractions that differ in size and maturity. These sporadic occurrences can significantly affect growers and buyers because a relatively small number of highly contaminated lots can lead to regulatory rejection, loss of export opportunities, and the need for costly segregation or disposal.

Kernel maturity, seed coat integrity, and physical damage are significant factors in susceptibility to contamination, with immature or damaged kernels often containing disproportionately high aflatoxin levels. Sorting and grading studies further show that contamination is frequently concentrated in smaller-sized and visually defective kernel fractions. Dorner et al. (1989) reported that immature peanut kernels were more likely to be contaminated than mature peanuts. Whitaker et al. (2005) showed that farmers' stock peanut size and color sorting can separate aflatoxin into smaller and poorer-quality fractions, supporting the idea that seed fraction can serve as an indicator of kernel vulnerability (Aoun et al., 2020; Mshanga et al., 2023).

Beyond field- and location-level variability, recent regional and national assessments indicate that short-term weather variability plays an important role in aflatoxin risk. Elevated temperatures during late pod filling, and rainfall deficits with prolonged dry periods have consistently been associated with increased contamination risk and greater likelihood of regulatory exceedance (Perrone et al., 2020).

Although substantial progress has been made in understanding aflatoxin ecology, this work has largely occurred at two separate scales: controlled, laboratory-based drought-simulation experiments and regional-scale monitoring datasets (Adeyeye, S. A. O. and Adeyeye, B. R., 2026). Comparatively little attention has been paid to how within-field heterogeneity such as seed maturity and size interacts with localized spatial variability and short-term environmental stress under commercial production conditions. Moreover, existing analyses typically characterize

average in-season trends or overall probabilities of exceedance, without explicitly distinguishing expected seasonal contamination patterns from unusual, anomalous peaks at individual sampling locations.

To address these gaps, this study developed an integrated analytical framework to:

(i) quantify in-season differences in aflatoxin contamination between larger and smaller peanut seed fractions;

(ii) characterize temporal patterns of aflatoxin contamination throughout the growing season and determine whether these patterns differ between seed fractions;

(iii) distinguish expected seasonal contamination patterns from unusually high or low contamination at individual sampling locations;

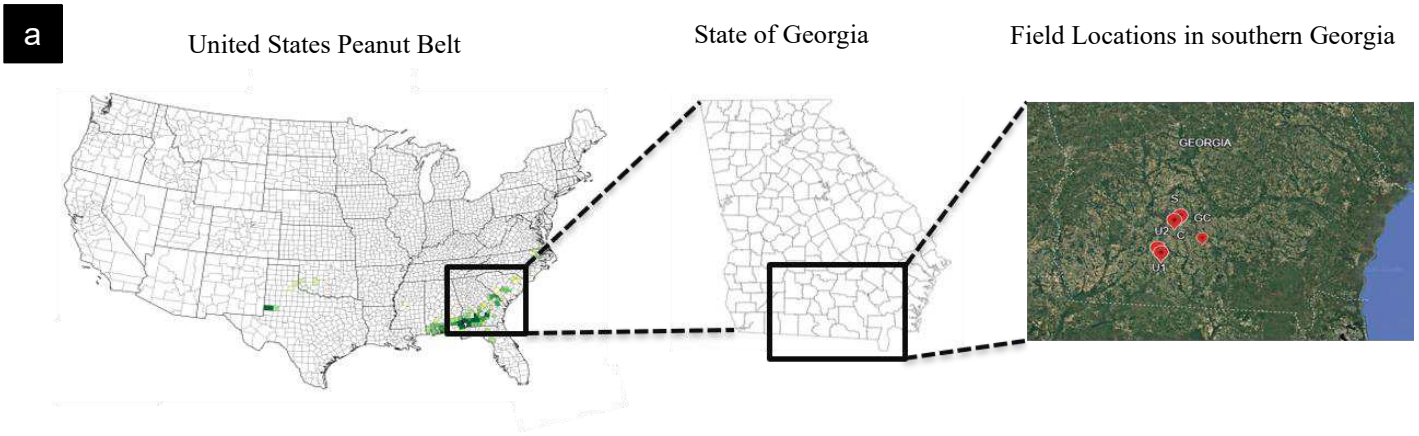
(iv) evaluate the extent to which measured environmental conditions explain variation in aflatoxin contamination and deviations from expected seasonal patterns; and

(v) identify the environmental factors most consistently associated with aflatoxin contamination and assess the extent to which these relationships are transferable across sampling locations and commercial fields.

2. Materials and Methods

2.1 Study Area

Five rainfed commercial peanut fields located in southern Georgia, U.S., were selected for data collection during the 2025 growing season (Figure 1a). Each field was divided into approximately 1-hectare grid cells to establish the sampling locations. Labeled points on the field maps in Figure 1b denote the center coordinates of the grid cells used for soil sampling and the point around which plant samples were collected for aflatoxin analyses. The five peanut fields were coded as C, GC, S, U1, and U2.



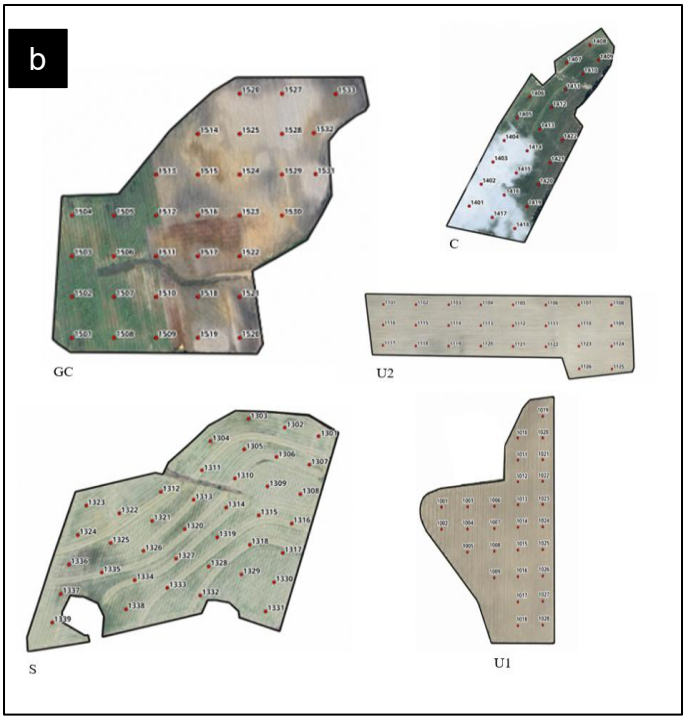


Figure 1. *(a) field locations across South Georgia, U.S.; (b) center point of grid cells across five fields.*

2.2 Sampling Design and Repeated Sampling Structure

Across all fields, a total of 148 fixed sampling locations were monitored throughout the growing season, including 22 in C, 33 in GC, 39 in S, 28 in U1, and 26 in U2. Each sampling location was intended to be sampled with four to five in-season sampling events. We began peanut pod sampling to measure aflatoxin levels at around 80 days after planting (DAP) and conducted 4 to 5 sampling events, the last one being at harvest, to observe the spatial and temporal fluctuations in contamination patterns. 5-6 peanut plants were sampled per plot per sampling event. The pods were detached, and oven dried at 60 ℃ for 24 h. Based on the literature, subsampling 25 g from 100 g of peanut seeds is adequate to detect aflatoxin concentrations with a reliable estimation (Luis, 2014). The dried samples were analyzed by Waters Agricultural Laboratory for aflatoxin concentrations using the Enzyme-linked immunosorbent assay (ELISA) method (Hidayat and Wulandari, 2021). At each sampling event, samples from each location were further split between two seed fractions (larger and smaller). This sampling design would yield 1,480 observations (148 sampling locations × 5 sampling events × 2 seed fractions). The final analysis dataset contained 1,475 observations because five observations were from the GC field were damaged and not used in the analyses.

In the laboratory, seeds were separated using a slotted screen with openings 6.35 mm wide × 19.05 mm long with seeds passing through the screen considered small seed fraction, and seeds retained on the screen considered larger seed fraction. In this study, the term paired refers to these two seed-fraction records originating from the same field, sampling location, and sampling event. Pairwise differences were calculated only when both fractions were available for the same sampling location-event combination. Seed-fraction class was assigned from the sample identifier.

Environmental predictor variables included weather, moisture-stress, soil, topographic, and spatial attributes (Table 1). Soil electrical conductivity (EC) was measured right before planting using Veris 3100 (Veris Technologies - Salina, KS) instrument. Intact 90 cm soil cores were collected at each grid center point shown in figure 1 (b). Each core was divided into six 15 cm increments and each increment was analyzed for texture (sand, silt, clay), organic matter content (OM), pH, cation exchange capacity (CEC), macronutrients (N, P, K, Ca, Mg), and micronutrients (Al) by Waters Agricultural Laboratories in Camilla, Georgia, United States. Topographic features, including mean elevation, relative elevation, and distance to the field edge, were calculated using ArcGIS Pro 3.3 (Esri, Redlands, CA, USA). Weather-derived predictors were calculated over pre-sampling windows ending on the sampling date. Weather observations were obtained from ATMOS 41W weather stations (METER Group, Pullman, WA, USA) installed at each field location, and daily variables were aggregated into 7-day and 14-day pre-sampling windows for subsequent analyses. For example, 7-day variables summarize conditions during the seven days immediately preceding and including the sampling date, whereas 14-day variables summarize the corresponding fourteen-day period. Aggregation was defined according to variable type: rainfall was summed over each window; dry days and days with maximum temperature above 35 °C were counted; and temperature and vapor pressure deficit (VPD) variables were summarized using their corresponding mean, minimum, or maximum values, as appropriate. Thus, the derived predictors represented cumulative precipitation, frequency of dry or high-temperature conditions, and characteristic thermal and atmospheric moisture-demand conditions immediately preceding each sampling event.

Table 1. *Variables included in the analysis and their definitions*

Category	**Variable**	**Description**	**Unit / Definition**
Seed / outcome variables	seed_class	Seed size class used for aflatoxin analysis	Categorical: larger or smaller seed fraction
	aflatoxin_ppb	Measured aflatoxin concentration	ppb (µg/kg)
	aflatoxin_detect	Indicator of whether aflatoxin was detected	Binary: 1 = detected; 0 = not detected
	aflatoxin_above_threshold	Indicator of whether aflatoxin concentration exceeded the specified regulatory/analytical threshold	Binary: 1 = above threshold; 0 = at or below threshold
Electrical conductivity / topography	Avg_Shallow_EC	Mean apparent soil electrical conductivity in the shallow soil layer	Dataset-specific EC unit
	Avg_Deep_EC	Mean apparent soil electrical conductivity in the deeper soil layer	Dataset-specific EC unit
	Avg_Elevation	Mean elevation of the sampling/field location	m

	Rel_Elevation_m	Relative elevation of the location within the field from the lowest elevation in the field	m
	Dist_To_Edge_m	Distance from the sampling location to the nearest field edge	m
Soil texture	sand_percent	Proportion of sand in the soil	%
	silt_percent	Proportion of silt in the soil	%
	clay_percent	Proportion of clay in the soil	%
Soil chemical properties	pH	Soil acidity/alkalinity	pH
	OM	Soil organic matter content	%
	CEC	Cation exchange capacity	cmolc kg^{-1}*
	Ca	Soil calcium concentration	ppm
	P	Soil phosphorus concentration	ppm
	N_percent	Soil nitrogen concentration	%
	K	Soil potassium concentration	ppm
	OC_percent	Soil organic carbon concentration	%
	NH4-N_ppm	Soil ammonium-N concentration	ppm
	NO3-N_ppm	Soil nitrate-N concentration	ppm
	Al_ppm	Soil aluminum concentration	ppm
	Mg ppm	Soil magnesium concentration	ppm
Weather: 7-day window	temp_max_7days	Maximum air temperature during the preceding 7 days	°C
	temp_min_7days	Minimum air temperature during the preceding 7 days	°C
	temp_mean_7days	Mean air temperature during the preceding 7 days	°C
	days_above35_7days	Number of days with temperature exceeding 35 °C during the preceding 7 days	days
	rain_7days	Cumulative precipitation during the preceding 7 days	mm
	dry_days_7d	Number of dry days during the preceding 7 days	days
	VPD_7days	Mean/summary vapor pressure deficit during the preceding 7 days	kPa*
Weather: 14-day window	temp_max_14days	Maximum air temperature during the preceding 14 days	°C
	temp_mean_14days	Mean air temperature during the preceding 14 days	°C
	rain_14days	Cumulative precipitation during the preceding 14 days	mm
	dry_days_14d	Number of dry days during the preceding 14 days	days

The raw aflatoxin distribution was right skewed and contained a small number of high concentrations. As a result, aflatoxin concentration was analyzed on the log1p scale as shown in Equation 1.

$$Y=\log\left(1+\text{aflatoxin}_{ppb}\right) \qquad (1)$$

The log1p transformation reduces the influence of these extreme values and improves model stability while preserving zero-valued observations. Because the transformation changes the scale of inference and may reduce sensitivity for some effects on the original ppb scale, inferential results are reported on the transformed scale, whereas raw-scale summaries are presented descriptively in Table 1. Figure 2 illustrates the transformed distribution of aflatoxin concentrations across the five sampling events for each field.

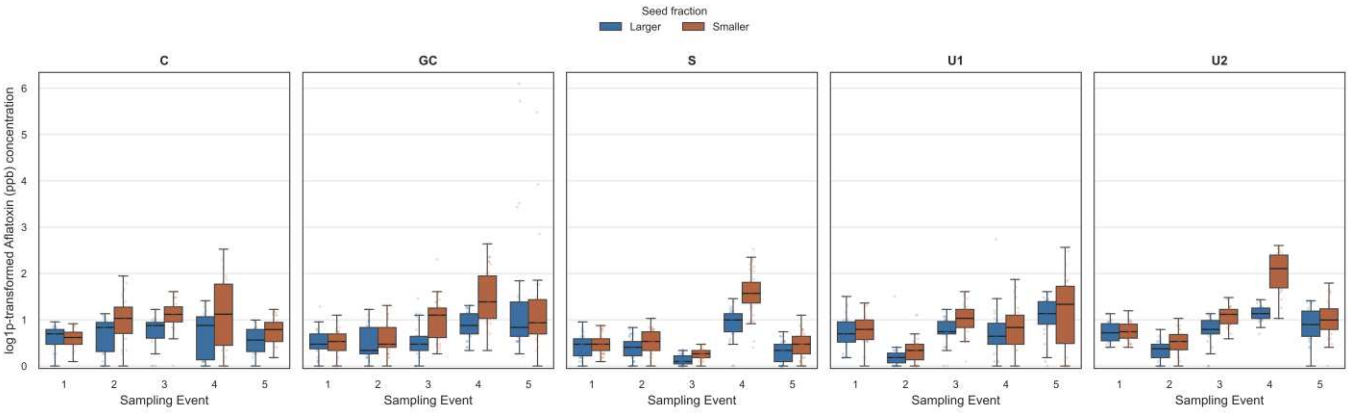


Figure 2. *Log-transformed aflatoxin distribution by field and sampling*

A summary of the dataset characteristics and repeated-sampling structure is provided in Table 2.

Table 2. *Dataset summary and repeated-measures structure*.

Item	Value
Usable aflatoxin observations	1,475
Commercial fields	5
Sampling locations	148
Sampling events per location	5
Seed fractions	larger, smaller
Median aflatoxin	1.00 ppb
Mean aflatoxin	2.18 ppb
Maximum aflatoxin	444.5 ppb
Observations >20 ppb*	6

* The U.S. FDA action level for total aflatoxins in foods intended for human consumption.

2.3 Analytical Workflow

The analytical workflow was designed to distinguish expected in-season contamination patterns from abnormal contamination behavior while preserving the repeated-measures structure of the dataset. The workflow combined inferential statistical modeling, nonlinear in-season trajectory

estimation, out-of-fold deviation analysis, and grouped machine-learning prediction to provide both biological interpretability and predictive insight (Figure 3).

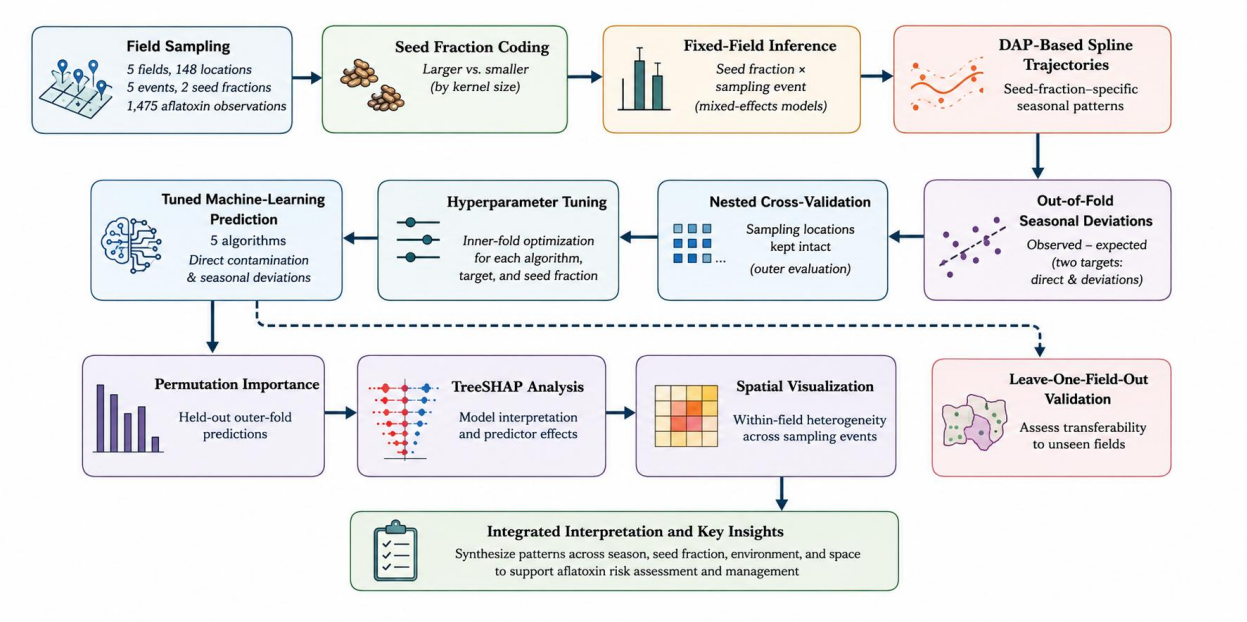


Figure 3. *Integrated analytical workflow.*

Data analysis proceeded in a stepwise fashion. First, to test whether contamination differences between larger and smaller seed fractions remained constant throughout the growing season or varied across sampling events, fixed-field statistical models were used. Second, to characterize how aflatoxin contamination changed continuously through the growing season and determine whether seasonal trajectories differed between seed fractions, spline regression models were fitted to log1p-transformed aflatoxin concentration. Third, to identify observations with contamination levels that were unusually high or low relative to their expected in-season pattern, out-of-fold in-season deviations were calculated using grouped cross-validation. Finally, to predict both direct contamination levels (in log1p aflatoxin) and in-season deviations, Random Forest, Extra Trees, Gradient Boosting, XGBoost, and Ridge regression models were evaluated separately for concentration (in log1p aflatoxin) and in-season deviation, and separately for larger and smaller seed fractions. Each analytical step is described in detail in the following sections.

To determine which measured environmental variables contributed most consistently to model predictions, the tuned machine-learning models were interpreted using permutation importance and XGBoost TreeSHAP. Permutation importance was used to quantify the loss in predictive performance after individual predictors were randomized, whereas TreeSHAP was used to evaluate the magnitude, direction, and nonlinear behavior of predictor contributions. Model transferability beyond the observed field system was additionally assessed using leave-one-field-out validation, in which each commercial field was held out in turn and model training and hyperparameter optimization were conducted using only the remaining fields.

2.4 Fixed-Field Statistical Models

To establish baseline in-season patterns and formally test seed-fraction differences, fixed-field statistical models were fitted to log1p-transformed aflatoxin concentration. The model included

field, seed fraction, sampling event, and the SeedFraction × SamplingEvent interaction as fixed effects. This structure allowed evaluation of whether contamination differences between larger and smaller seed fractions remained constant throughout the season or varied across sampling events. Field was treated as a fixed effect because the objective of the study was to compare the five specific commercial fields included in the dataset rather than generalize to a broader population of fields. Repeated observations collected from the same sampling location were accounted for using cluster-robust standard errors clustered by sampling location. This approach allows observations within a sampling location to exhibit correlated errors rather than assuming independence among repeated measurements, while retaining the fixed-effects model structure (Cameron and Miller, 2015). The primary inferential model can be expressed as:

$$Y_{ijk} = \beta_0 + \beta_1(Field) + \beta_2(Seed\ Fraction) + \beta_3(Sampling\ Event) + \beta_4(Seed\ Fraction \times Sampling\ Event) + \epsilon_{ijk}$$

where $Y_{ijk}$is the log1p-transformed aflatoxin concentration and, and $\epsilon_{ijk}$is the residual error term. To determine whether in-season contamination patterns differed between seed fractions, the full model containing the SeedFraction × SamplingEvent interaction was compared with a reduced model containing only the corresponding main effects. Fixed-effect significance was evaluated using cluster-robust Wald tests.

An additional environmentally adjusted model was fitted as a sensitivity analysis. Prior to model fitting, candidate environmental, soil, and topographic predictors were screened for multicollinearity using pairwise correlation analysis and variance-inflation diagnostics. When highly redundant predictors were identified, only the less collinear predictors were retained in the adjusted model. Residual diagnostics were evaluated to assess model assumptions and overall model adequacy.

2.5 Estimation of Expected In-Season Contamination Trajectories

Because in-season contamination patterns were not expected to follow simple linear trends, spline-based regression models were used to estimate nonlinear in-season contamination trajectories. These models were designed to characterize expected contamination dynamics while allowing in-season responses to vary between seed fractions.

In-season timing was represented using DAP as the primary continuous measure of crop development. DAP was selected because sampling events were not collected on identical calendar dates across all fields and because crop developmental timing is more biologically meaningful than event number when describing in-season contamination processes.

The spline model included field effects, seed fraction, and a seed-fraction-by-time spline interaction, allowing in-season trajectories to differ between larger and smaller seed fractions. Cubic regression splines were used to estimate smooth nonlinear contamination patterns across the growing season. The general form of the model was:

$$Y_i = \beta_0 + \beta_1(\text{Field}) + \beta_2(\text{Seed Fraction}) + s(\text{DAP}) + s(\text{DAP}) \times \text{Seed Fraction} + \varepsilon_i$$

where Y_i represents the observed log1p-transformed aflatoxin concentration, $s(\text{DAP})$is a cubic spline function describing nonlinear in-season progression, and $\varepsilon_i$is the residual error term. The resulting spline trajectories were interpreted as estimates of expected in-season contamination

progression and were subsequently used to derive out-of-fold in-season deviations for downstream analyses.

To assess whether the primary seed-fraction findings were disproportionately influenced by any single field, a leave-one-field-out inferential sensitivity analysis was conducted. The fixed-field SeedFraction × SamplingEvent model and the DAP-based spline model were each refitted five times, with one field omitted in each iteration. Global interaction tests, within-event seed-fraction contrasts, and fitted trajectory differences were then compared with the corresponding full-data results.

2.6 Out-of-Fold In-Season Deviations

To separate expected in-season contamination patterns from abnormal contamination behavior, out-of-fold in-season deviations were calculated using grouped validation, with sampling location used as the grouping unit. Under this approach, all observations from the same sampling location, including repeated sampling events and both seed fractions, were assigned to the same validation fold. This prevented observations from the same location from being used simultaneously for model fitting and validation. The objective was to identify contamination levels that were unusually high or low relative to the expected in-season trajectory for a given sampling location and seed fraction.

The 148 sampling locations were partitioned into five grouped validation folds, providing approximately 80% of the locations for model fitting and 20% for validation in each iteration. Folds were constructed at the sampling-location level and could contain locations from multiple fields. Once a sampling location was assigned to a fold, all observations from that location including both seed fractions and all repeated sampling events remained in the same fold. Thus, no observation from a held-out sampling location was available to the model during fitting. The purpose of this design was to evaluate model performance for sampling locations not used during model fitting while preventing information leakage arising from repeated measurements from the same location. Accordingly, grouped five-fold validation estimates generalization to new sampling locations within the observed field system rather than transferability to an entirely unseen field. Transferability across fields was evaluated separately using leave-one-field-out validation.

For each validation fold:

1. the DAP-based spline regression model was fitted using the training folds,
2. expected contamination values were predicted for the held-out sampling locations, and
3. in-season deviations were calculated as:

$$D_i = Y_i - \hat{Y}_i^{(-k)}$$

where $D_i$is the in-season deviation, $Y_i$is the observed log1p-transformed aflatoxin concentration, and $\hat{Y}_i^{(-k)}$is the expected in-season value predicted for observation i using a spline model fitted without the validation fold containing that observation.

Positive deviation values indicate contamination levels higher than expected given the in-season timing, field context, and seed-fraction-specific trajectory, whereas negative values indicate contamination levels lower than expected. Because expected values were generated from models fitted without the corresponding validation observations, the resulting in-season deviations provide an independent measure of abnormal contamination behavior relative to the estimated in-season pattern.

2.7 Machine-Learning Analysis

Following estimation of expected in-season structure, machine-learning models were used to identify environmental predictors associated with both direct contamination levels and in-season deviations. Two prediction targets were defined:

- Direct contamination, corresponding to log1p-transformed aflatoxin concentration;
- In-season deviation, representing departures from the expected in-season contamination trajectory.

Models were fitted separately for larger and smaller seed fractions to allow fraction-specific relationships between environmental conditions and contamination risk. The evaluated algorithms included Random Forest (RF; Breiman, 2001), Extra Trees (ET; Geurts et al., 2006), Gradient Boosting Machine (GBM; Friedman, 2001), Extreme Gradient Boosting (XGBoost; Chen and Guestrin, 2016), and Ridge regression (Hoerl and Kennard, 1970).

Model performance was evaluated using nested five-fold cross-validation with sampling location as the grouping unit. The 148 sampling locations were partitioned among five outer validation folds, with all repeated observations from a given location, including both seed fractions and all sampling events kept together. Thus, approximately one-fifth of the sampling locations were held out for evaluation in each outer iteration, while the remaining locations were used for model training and inner hyperparameter optimization. This design evaluated prediction at sampling locations not used for model fitting while preventing information leakage among repeated observations. Because the held-out folds contained sampling locations from the observed fields, this procedure assessed generalization to new locations within the observed field system. Transferability to an entirely unseen field was evaluated separately using leave-one-field-out validation. Missingness was assessed for all candidate predictors before model fitting. Predictors without missing observations were not imputed. For predictors containing missing values, missing observations were replaced with the median calculated exclusively from the corresponding training fold. The same training-fold median was then applied to the held-out validation observations. Predictor standardization was performed using the same training-fold-only procedure.

Model hyperparameters were optimized using nested cross-validation rather than prespecified values. For each prediction target and seed fraction, the outer five-fold cross-validation was used exclusively for model evaluation, while hyperparameter optimization was conducted within the corresponding outer training data using inner cross-validation grouped by sampling location. Random Forest and Extra Trees models were tuned across tree number, maximum tree depth, minimum samples required for splitting and terminal leaves, and the number of predictors considered at each split. Gradient Boosting models were tuned across the number of boosting iterations, learning rate, tree depth, minimum split and leaf sizes, subsampling fraction, and feature sampling. XGBoost models were tuned across the number of boosting iterations, learning rate, maximum tree depth, minimum child weight, row and column subsampling, minimum loss reduction, and L1 and L2 regularization. Ridge regression was tuned across a broad range of regularization strengths. Hyperparameter combinations were selected by minimizing root mean square error (RMSE) within the inner cross-validation procedure. The selected configuration was then refitted using the complete outer training set and evaluated on the held-out outer fold. Final performance metrics were calculated exclusively from pooled outer-fold predictions, ensuring that

observations used for model evaluation did not contribute to either model fitting or hyperparameter selection.

Predictive performance of the tuned models was quantified using RMSE, mean absolute error (MAE), coefficient of determination (R^2), and Spearman rank correlation. Hyperparameter optimization was conducted exclusively within the inner training folds, and performance was evaluated on the corresponding held-out outer folds. Final performance metrics were calculated from pooled outer-fold predictions across the five outer validation folds, providing an out-of-sample assessment that was independent of both model fitting and hyperparameter selection.

Environmental-driver interpretation was performed using permutation importance and XGBoost TreeSHAP applied to the tuned machine-learning models. Permutation importance quantified the decrease in held-out predictive performance resulting from random permutation of each predictor, thereby providing a model-based measure of predictor importance. TreeSHAP was applied to the tuned XGBoost models to characterize the magnitude and direction of individual predictor contributions and to identify nonlinear relationships between environmental conditions and model predictions.

3. Results

3.1 Fixed-Field Evidence for In-Season Seed-Fraction Divergence

Fixed-field Wald tests demonstrated significant effects of seed fraction, sampling event, and field on log1p-transformed aflatoxin concentration (Table 3). Seed fraction was significant as a main effect ($\chi^2 = 4.246$, df = 1, $p = 0.039$), indicating overall contamination differences between larger and smaller fractions. Sampling event ($\chi^2 = 151.584$, df = 4, $p < 0.001$) and field ($\chi^2 = 169.491$, df = 4, $p < 0.001$) were also highly significant, demonstrating substantial temporal and field-level variation in contamination levels. Most importantly, a highly significant SeedFraction × SamplingEvent interaction was detected ($\chi^2 = 147.364$, df = 4, $p < 0.001$), indicating that contamination differences between larger and smaller seed fractions varied across sampling events rather than remaining constant throughout the growing season.

Table 3. *Fixed-effect Wald tests for field, seed fraction, sampling event, and seed fraction and sampling event interaction.*

Effect	Wald χ^2	df	p value
Seed fraction	4.246	1	0.039
Sampling event	151.584	4	<0.001
Field	169.491	4	<0.001
Seed fraction × Sampling event	147.364	4	<0.001

Seed-fraction differences varied across sampling events (Figure 4). The smaller seed fraction had significantly higher aflatoxin concentrations during sampling events 2, 3, and 4, whereas no significant differences were detected during events 1 and 5. The greatest separation between fractions occurred during sampling event 4.

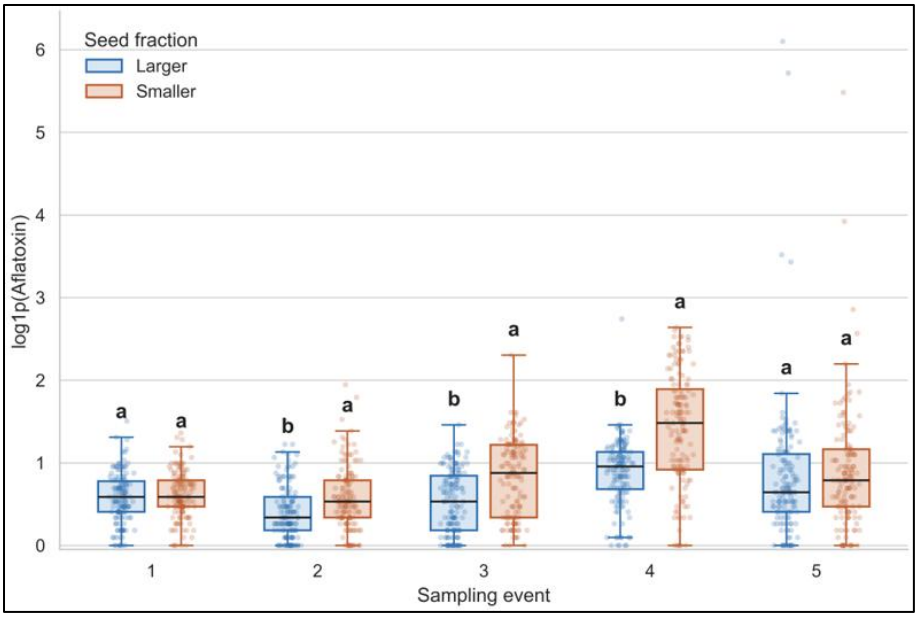


Figure 4. *Log1p-transformed aflatoxin concentrations by seed fraction and sampling event. Different letters indicate significant within-event differences between seed fractions (Holm-adjusted $p < 0.05$).*

Pairwise comparisons using Holm-adjusted p-values confirmed that contamination in the smaller fraction was significantly greater than contamination in the larger fraction during sampling events 2, 3, and 4 (Holm-adjusted $p < 0.001$). The largest difference occurred during sampling event 4, where the estimated mean difference between fractions was 0.537 log1p units. In contrast, contamination differences were not statistically significant during sampling event 1 (Holm-adjusted $p = 0.079$) or sampling event 5 (Holm-adjusted $p = 0.092$). These results indicate that seed-fraction divergence was concentrated within specific in-season periods rather than occurring uniformly throughout the growing season.

Figure 5 illustrates the in-season progression of mean log1p-transformed aflatoxin contamination across sampling events for the two seed fractions. Contamination levels were relatively similar early in the season but diverged substantially during the mid-to-late season, particularly during sampling event 4, when contamination increased more rapidly in the smaller fraction. The reduced difference observed during the final sampling event is consistent with the non-significant pairwise comparison observed for event 5.

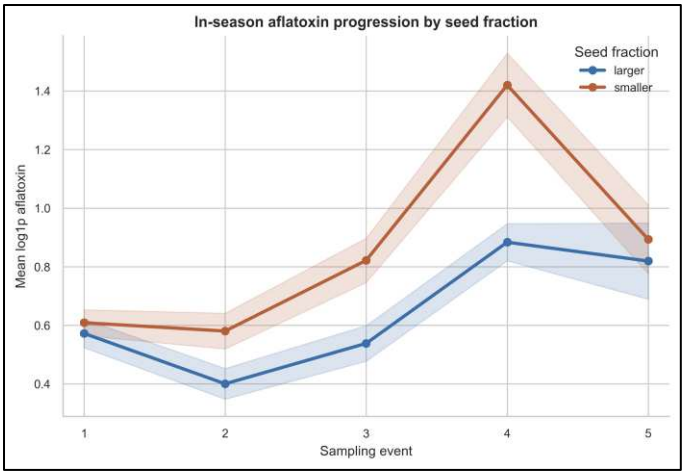


Figure 5. *In-season progression of log1p-transformed aflatoxin contamination by seed fraction across in-season sampling events. Points represent event-level means, and shaded bands represent confidence intervals.*

To further evaluate how seed-fraction differences varied across fields and sampling events, within-location paired differences were calculated as the aflatoxin concentration of the smaller fraction minus the corresponding concentration of the larger fraction from the same field, sampling location, and sampling event. The resulting heatmap (Figure 6) revealed substantial temporal and field-level heterogeneity in seed-fraction divergence. Positive values indicate greater contamination in the smaller fraction, whereas negative values indicate greater contamination in the larger fraction.

The largest positive differences were concentrated during sampling event 4, particularly within the U2 and S fields, demonstrating that contamination became increasingly concentrated within the smaller fraction during specific in-season windows. These patterns support the inferential results by showing that seed-fraction effects were episodic and field-dependent rather than constant across the growing season.

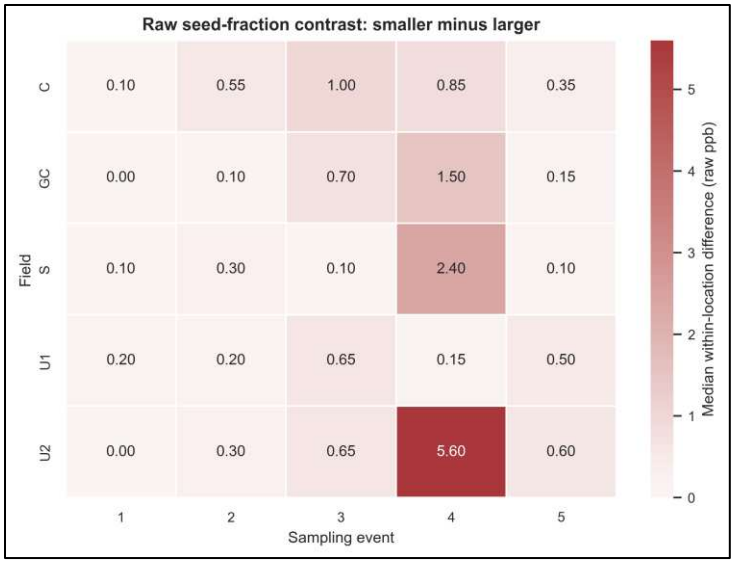


Figure 6. *Median within-location seed-fraction difference in aflatoxin contamination(ppb), calculated as smaller fraction minus larger fraction for records originating from the same field, sampling location, and sampling event. Positive values indicate higher contamination in the smaller seed fraction.*

3.2 Nonlinear In-season Contamination Trajectories

DAP-based spline regression models revealed nonlinear seasonal contamination patterns rather than a simple monotonic increase throughout the growing season. The estimated trajectories indicated that contamination risk increased during specific developmental periods and subsequently declined, suggesting that contamination accumulation was concentrated within discrete seasonal windows rather than progressing uniformly over time.

Figure 7 shows the observed log1p-transformed aflatoxin concentrations together with fitted DAP-based spline trajectories from a joint model that included both seed fractions and a seed-fraction-by-DAP spline interaction. This joint modeling structure allowed formal evaluation of whether the seasonal contamination trajectory differed between larger and smaller seed fractions. The fitted trajectory for the smaller seed fraction increased more steeply during the primary contamination-risk period and reached a higher fitted peak than the larger seed fraction, whereas the larger fraction showed a more gradual seasonal response.

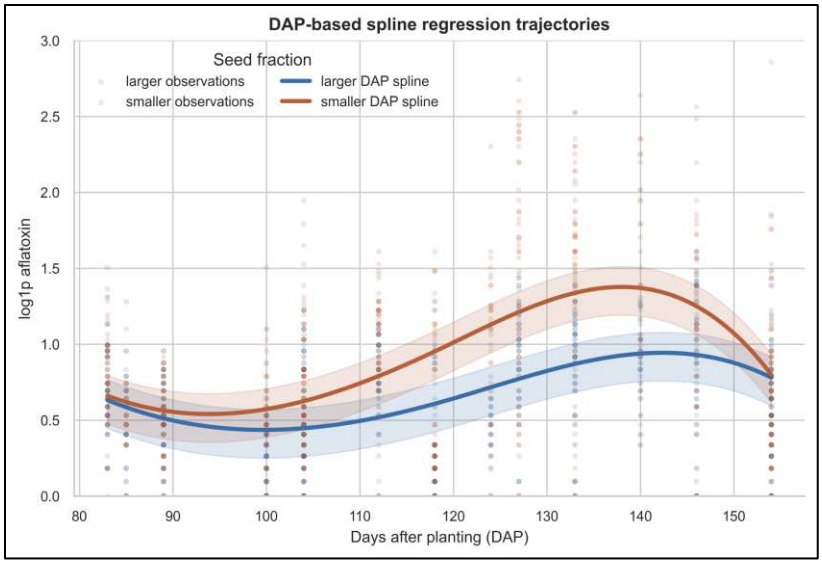


Figure 7. *DAP-based spline trajectories of log1p-transformed aflatoxin concentration by seed fraction. The y-axis is restricted to 0-3 for visualization; all observations were retained in model fitting.*

To test whether the two fitted in-season trajectories differed, a Wald test was performed on the seed-fraction-by-DAP spline interaction term. The interaction was highly significant ($\chi^2 = 120.226$, df = 4, $p < 0.001$), indicating that the overall DAP-based seasonal trajectory differed significantly between larger and smaller seed fractions (Table 4). This test evaluates whether the shape of the seasonal trajectory differs between seed fractions across the DAP range; it should not be interpreted as a separate pointwise test of seed-fraction differences at each individual DAP value.

Table 4. *Global Wald test of seed-fraction-by-DAP spline interaction. The test evaluates whether the fitted seasonal contamination trajectories differ between larger and smaller seed fractions across the DAP range.*

Effect	Wald χ^2	df	p value
Seed fraction × DAP spline trajectory	120.226	4	<0.001

These results indicate that contamination dynamics varied not only through time but also between seed fractions. The significant spline interaction supports the interpretation that seasonal contamination progression was fraction-specific and justifies the use of fraction-specific fitted seasonal trajectories when estimating expected contamination patterns and deriving seasonal deviations for subsequent analyses.

A leave-one-field-out sensitivity analysis showed that the principal seed-fraction pattern was not driven by any single field. Both the SeedFraction × SamplingEvent interaction and the SeedFraction × DAP spline interaction remained statistically significant after each of the five fields was omitted individually. The direction of the smaller-minus-larger contrast during sampling events 2–4 was also retained across all field omissions. The largest change in the event-4 contrast occurred after omission of U1, differing from the full-data estimate by 0.107 log1p units, while the largest change in peak fitted spline separation was 0.091 log1p units. These results indicate that the mid-season seed-fraction divergence and the overall difference in

season trajectories were robust to the influence of individual fields.

3.3 Out-of-Fold In-Season Deviations from Expected Contamination

Out-of-fold in-season deviation analysis separated expected in-season contamination patterns from abnormal contamination behavior at individual sampling locations. For each observation, expected contamination was estimated using DAP-based spline regression models fitted without information from the corresponding validation fold. In-season deviation was then calculated as the observed log1p-transformed aflatoxin concentration minus the corresponding out-of-fold expected value.

Figure 8 summarizes the resulting in-season deviations. Positive deviation values indicate contamination levels higher than expected given the in-season timing, field context, and seed-fraction-specific in-season trajectory, whereas negative values indicate contamination levels lower than expected.

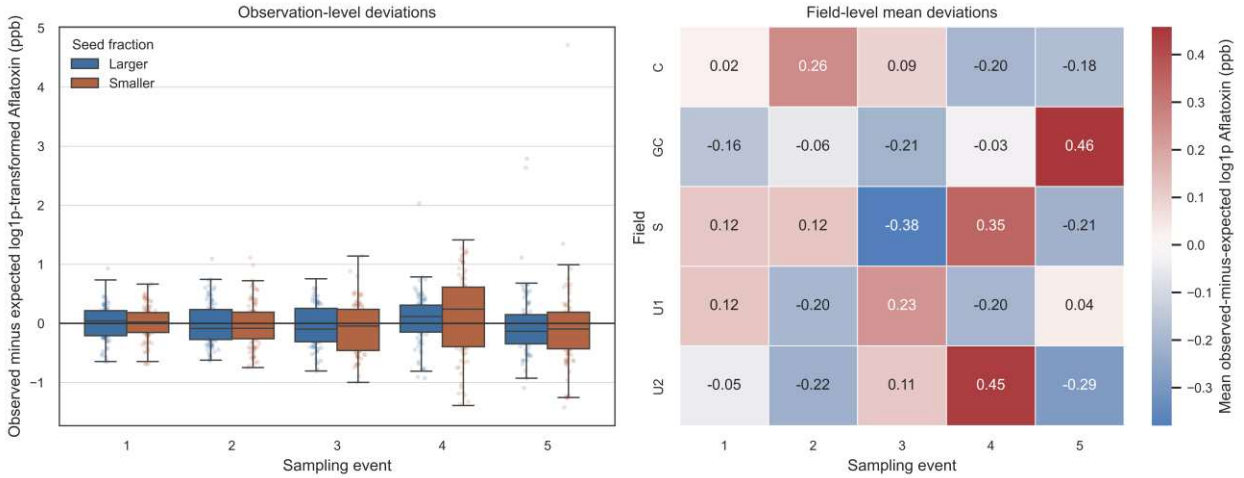


Figure 8. *Out-of-fold in-season deviations from expected contamination. Boxplots (left figure) show observation-level deviations by sampling event and seed fraction, and the heatmap (right figure) shows field-level mean deviations.*

Observation-level distributions revealed substantial variability around the expected in-season trajectories, with both positive and negative deviations occurring throughout the growing season. Field-level summaries further demonstrated that deviation patterns were not uniformly distributed among fields, indicating localized contamination behavior that could not be explained solely by in-season progression.

Positive deviations identified sampling-location and sampling-event combinations exhibiting contamination levels substantially above the expected in-season pattern. In contrast, negative deviations represented observations with lower contamination than expected for the corresponding in-season stage. By separating expected in-season progression from unusual contamination behavior, this analysis distinguished ordinary in-season increases from abnormal contamination spikes that may be particularly relevant for field-level monitoring and risk-management applications.

3.4 Machine-Learning Prediction Performance Under Grouped Validation

Machine-learning performance was evaluated using nested five-fold cross-validation with sampling location as the grouping unit. Hyperparameters were optimized within the inner training folds, whereas the outer folds were reserved exclusively for model evaluation. Final performance metrics were calculated from pooled predictions for the held-out outer folds.

Comparison across the five tuned algorithms showed that tree-based ensemble models generally achieved lower held-out RMSE than Ridge regression, although differences among the leading ensemble methods were relatively small (Figure 9). The performance of the best-performing models is summarized in Table 5. For direct contamination, Random Forest provided the lowest RMSE for both seed fractions. For in-season deviation, Extra Trees provided the lowest RMSE for both fractions.

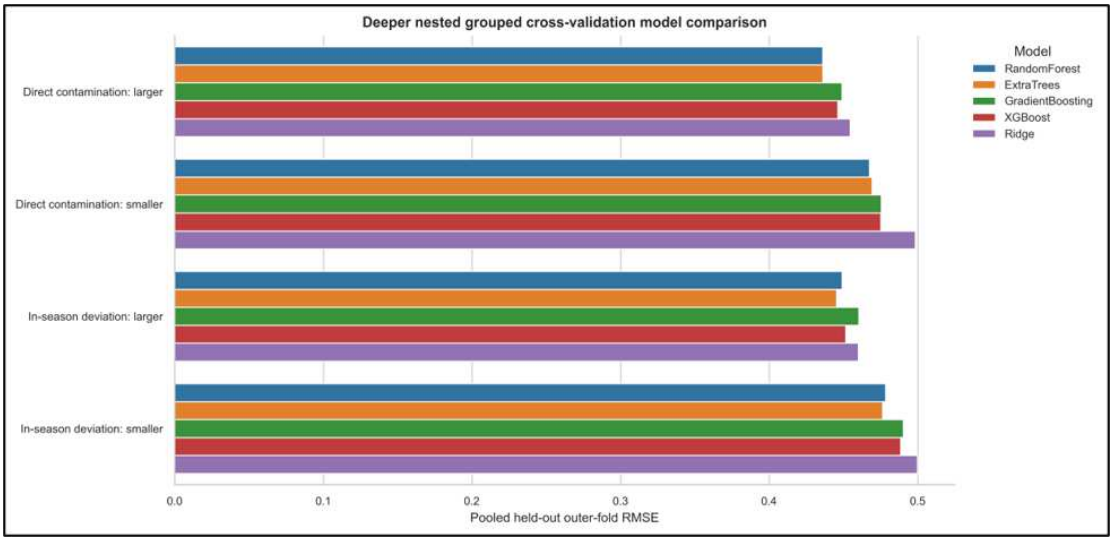


Figure 9. *Comparison of tuned machine-learning models based on pooled held-out outer-fold RMSE for each prediction target and seed fraction.*

Table 5. *Best-performing tuned machine-learning models under nested cross-validation*

Prediction target	Seed fraction	Best model	RMSE	MAE	R^2	Spearman
Direct contamination	Larger	Random Forest	0.436	0.273	0.271	0.616
Direct contamination	Smaller	Random Forest	0.467	0.322	0.416	0.655
In-season deviation	Larger	Extra Trees	0.445	0.279	0.109	0.434
In-season deviation	Smaller	Extra Trees	0.476	0.326	0.186	0.479

Note: Models were selected based on pooled held-out outer-fold RMSE after hyperparameter optimization within the inner cross-validation folds. Direct contamination represents log1p-transformed aflatoxin concentration; in-season deviation represents departure from the corresponding out-of-fold expected seasonal trajectory.

For direct contamination, predictive performance was higher for the smaller seed fraction (R^2 = 0.416) than for the larger fraction (R^2 = 0.271). Prediction of in-season deviations was more difficult, with the best-performing models explaining 10.9% and 18.6% of the variation in the larger and smaller fractions, respectively. Thus, removal of the expected in-season trajectory substantially reduced the amount of variation that could be predicted from the measured environmental and spatial variables.

Observed-versus-predicted relationships from the held-out outer folds further illustrate these differences (Figure 10). Predictions followed the observed contamination gradient more closely for direct contamination than for in-season deviations. Prediction errors increased for relatively rare high-contamination observations, indicating that extreme contamination events remained difficult to predict even after hyperparameter optimization.

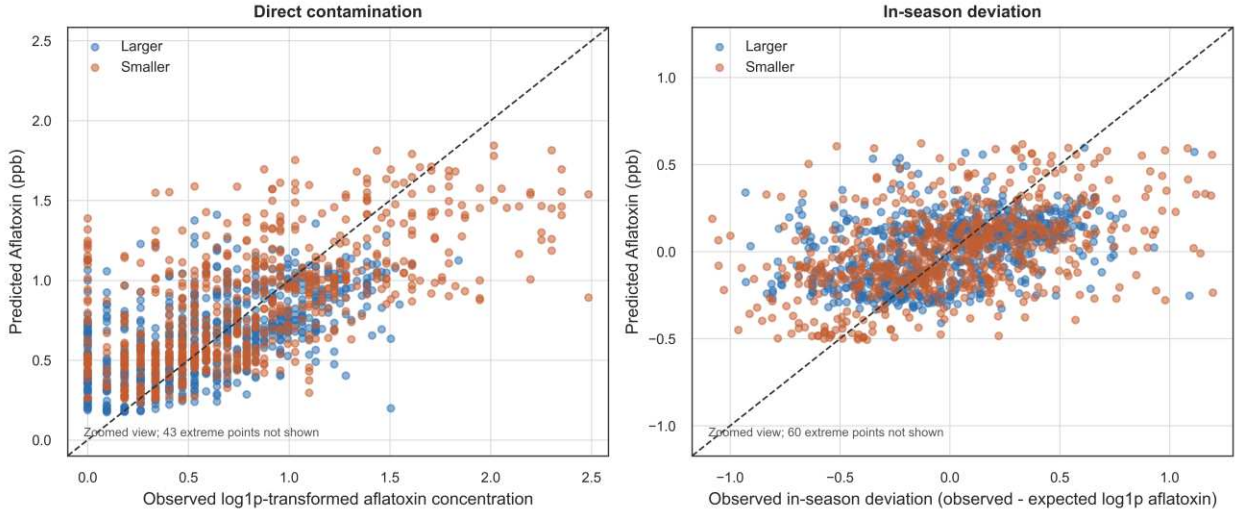


Figure 10. *Observed versus out-of-fold predicted values from tuned machine-learning models under nested cross-validation. The dashed line represents the 1:1 relationship. Axes were restricted for visualization; extreme observations were retained in model training and performance evaluation.*

To evaluate model transferability beyond sampling-location validation, leave-one-field-out analyses were conducted as a sensitivity assessment (Supplementary Table S1). Predictive performance generally declined under field-level holdout, indicating that prediction for previously unseen fields was substantially more difficult than prediction for held-out sampling locations within the observed field system. These results suggest that environmental predictors contain meaningful information regarding both contamination levels and in-season deviations, but field-specific variability remains an important source of uncertainty.

3.5 Environmental Drivers of Direct Contamination and In-Season Deviations

Permutation importance calculated from the held-out outer folds of the tuned models identified short-term moisture and thermal conditions as the most consistent environmental signals associated with both direct aflatoxin contamination and in-season deviations (Figure 11). Across prediction targets and seed fractions, dry-day accumulation, recent rainfall, and temperature metrics repeatedly ranked among the most influential predictors.

For direct contamination, dry_days_7d, rain_7days, temp_min_7days, temp_max_7days, and temp_mean_7days were among the recurring high-ranking predictors. The relative importance of individual variables differed between the larger and smaller seed fractions, indicating that the environmental information associated with contamination was not identical between fractions.

After removal of the expected in-season trajectory, moisture and thermal variables remained important for predicting in-season deviations. Rainfall over the 7- day windows, dry-day accumulation, and recent temperature conditions continued to contribute predictive information, although their rankings varied between seed fractions. The persistence of these variables after accounting for the expected seasonal pattern indicates that short-term environmental conditions were associated not only with overall contamination levels but also with departures from expected in-season contamination behavior.

Topographic and soil-related variables, including average elevation and soil pH, also appeared among the higher-ranked predictors in some model panels, but their importance was less consistent across targets and seed fractions than that of the short-term weather variables. Predictor importance should therefore be interpreted as model-based predictive contribution rather than evidence of a direct causal effect.

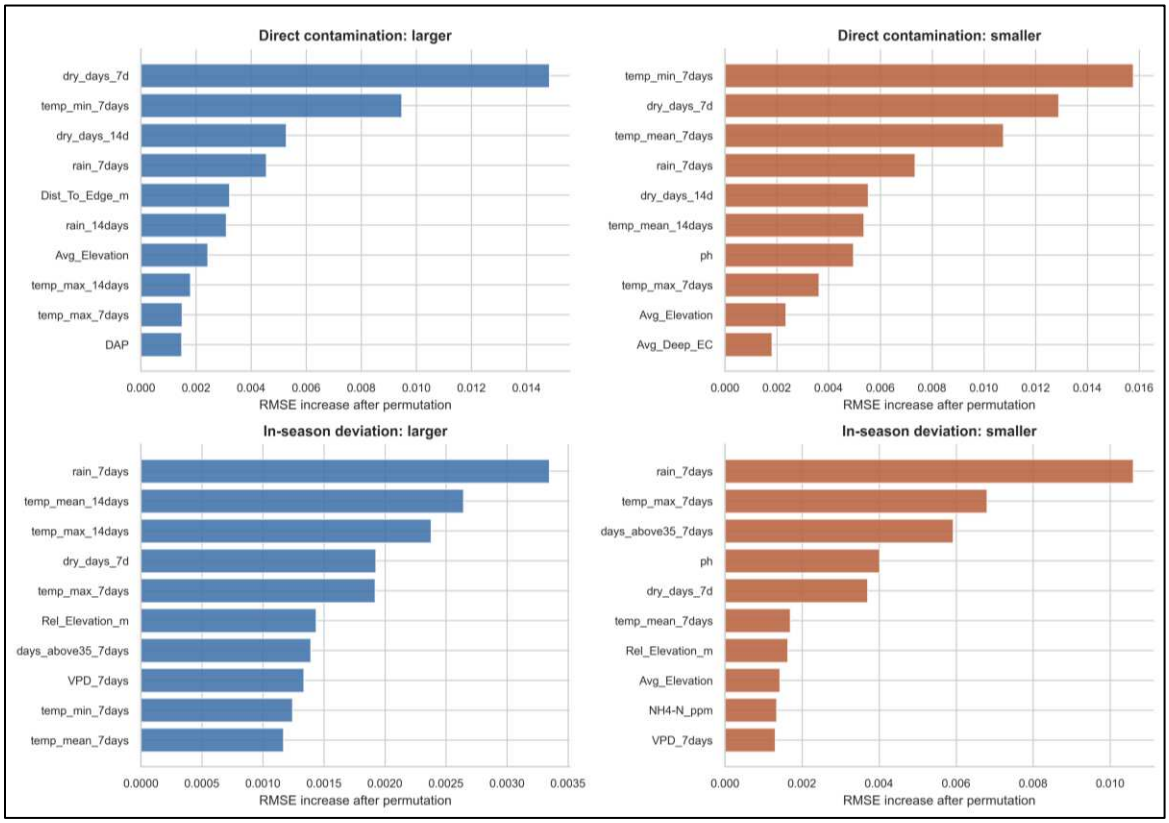


Figure 11. *Held-out outer-fold permutation importance from tuned models for direct contamination (top graphs) and in-season deviation (bottom graphs). Importance represents the increase in RMSE after predictor permutation.*

3.6 Consensus Variable Importance Across Prediction Targets

To identify environmental predictors that remained consistently important across prediction targets and seed fractions, consensus importance was summarized from the held-out outer-fold permutation-importance results. This analysis distinguished predictors that repeatedly contributed predictive information across multiple model panels from those whose importance was specific to a particular seed fraction or prediction target. The scaled importance profiles revealed distinct predictor patterns among the four modeling contexts (Figure 12). Direct

contamination in the larger fraction was most strongly characterized by short-term dry conditions, whereas minimum temperature was more prominent in the smaller fraction. In contrast, recent rainfall showed the strongest relative importance for in-season deviations in both seed fractions. Temperature-related predictors were particularly prominent for the larger-fraction deviations, while extreme-heat indicators contributed more strongly to smaller-fraction deviations. These contrasts indicate that the relative influence of environmental predictors depended on both the prediction target and seed fraction.

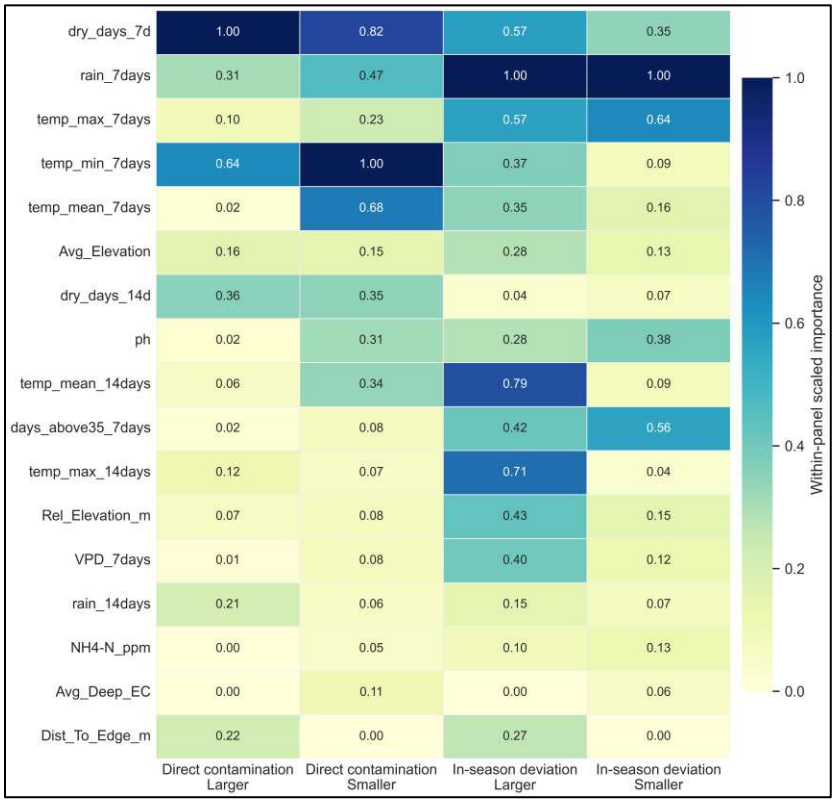


Figure 12. *Consensus permutation importance across prediction targets and seed fractions. Values represent within-panel scaled importance calculated from held-out outer-fold predictions after nested hyperparameter tuning.*

Short-term moisture and temperature variables showed the greatest consistency (Table 6). dry_days_7d and rain_7days were among the top-ranked predictors in all four target-by-fraction panels, while temp_max_7days also appeared among the top predictors across all four panels. temp_min_7days and temp_mean_7days were among the top-ranked predictors in three of four panels. Longer-term variables, including dry_days_14d, temp_mean_14days, and temp_max_14days, provided additional but less consistent predictive information.

Non-weather predictors were less consistently represented. Average elevation appeared among the top predictors in three panels, whereas soil pH and relative elevation appeared in two panels. Overall, the consensus analysis indicates that short-term moisture availability and thermal conditions immediately preceding sampling provided the most reproducible environmental signals across prediction targets and seed fractions.

Table 6. *Consensus environmental predictor importance from held-out outer-fold permutation importance.*

Predictor	Mean importance	Best rank	Top 10 evidence count	Panels present	Biological interpretation
dry_days_7d	0.008	1	4	4	Short-term rainfall deficit and moisture stress
rain_7days	0.006	1	4	4	Recent rainfall conditions before sampling
temp_max_7days	0.003	2	4	4	Recent maximum-temperature exposure
temp_min_7days	0.007	1	3	4	Recent minimum-temperature regime
temp_mean_7days	0.003	3	3	4	Recent mean-temperature regime
Avg_Elevation	0.002	7	3	4	Topographic position and drainage context
dry_days_14d	0.003	3	2	4	Extended dry period before sampling
pH	0.003	4	2	4	Soil acidity and nutrient-availability context
temp_mean_14days	0.002	2	2	4	Two-week thermal background
days_above35_7days	0.002	3	2	4	Recent extreme-heat frequency
temp_max_14days	0.001	3	2	4	Two-week maximum-temperature background
Rel_Elevation_m	0.001	6	2	4	Relative microtopographic position
VPD_7days	0.001	8	2	4	Atmospheric drying demand
rain_14days	0.001	6	1	4	Two-week rainfall context

3.7 TreeSHAP Interpretation of Environmental Effects

TreeSHAP analysis was used to examine how individual predictor values contributed to the tuned XGBoost predictions (Figure 13). Unlike permutation importance, which quantifies the overall predictive relevance of a variable, TreeSHAP provides information on both the magnitude and direction of its contribution.

The contribution patterns differed substantially among prediction targets and seed fractions. For direct contamination, dry_days_7d and temp_min_7days had the largest mean absolute TreeSHAP values in the larger fraction, whereas temp_min_7days, rain_7days, and temp_mean_7days dominated the smaller fraction. For in-season deviations, the larger fraction was characterized primarily by rain_14days, temp_mean_14days, and dry_days_14d, while rain_7days, dry_days_14d, and temp_max_7days were most influential in the smaller fraction.

The TreeSHAP distributions also showed that predictor contributions were not uniformly linear or consistent in direction across the four modeling contexts. Thus, the environmental conditions associated with predicted contamination depended on both seed fraction and whether the model targeted overall contamination or departures from the expected seasonal trajectory.

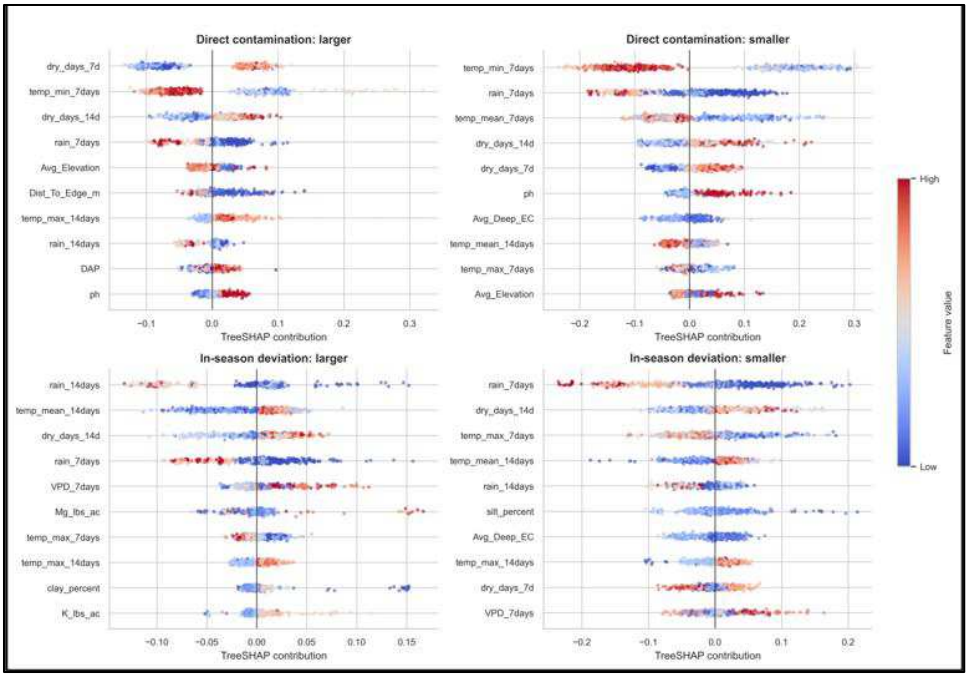


Figure 13. *TreeSHAP contributions from tuned XGBoost models for direct contamination and in-season deviations. Point color represents relative predictor values.*

3.8 Spatial and Field-Level Heterogeneity

Spatial visualization showed substantial within-field variation in aflatoxin contamination across sampling events (Figure 14). Measured aflatoxin concentrations were spatially interpolated using Empirical Bayesian Kriging (EBK) in ArcGIS Pro 3.3 (Esri, Redlands, CA, USA.). EBK was performed using the measured aflatoxin concentration as the z-value field, with no data transformation applied. A maximum of 100 observations was used for each local model, with a local model area overlap factor of 1 and 100 simulated semivariograms. A smooth circular search neighborhood with a radius of 143.16 m and a smoothing factor of 0.2 was used. A power semivariogram model was specified, and the output surface represented predicted aflatoxin concentrations. The resulting prediction raster was constrained to the field boundary.

Contamination was spatially heterogeneous, with areas of relatively low and elevated aflatoxin occurring within the same field and changing across successive sampling events.

The spatial patterns also differed between seed fractions. Elevated contamination became more spatially extensive during later sampling events in one fraction, whereas the corresponding pattern in the other fraction remained more localized. These observations complement the temporal and predictive analyses by demonstrating that aflatoxin contamination varied not only through the growing season but also among locations within the field. Because these maps are descriptive, the apparent spatial patterns were not interpreted as evidence of statistically significant spatial clustering.

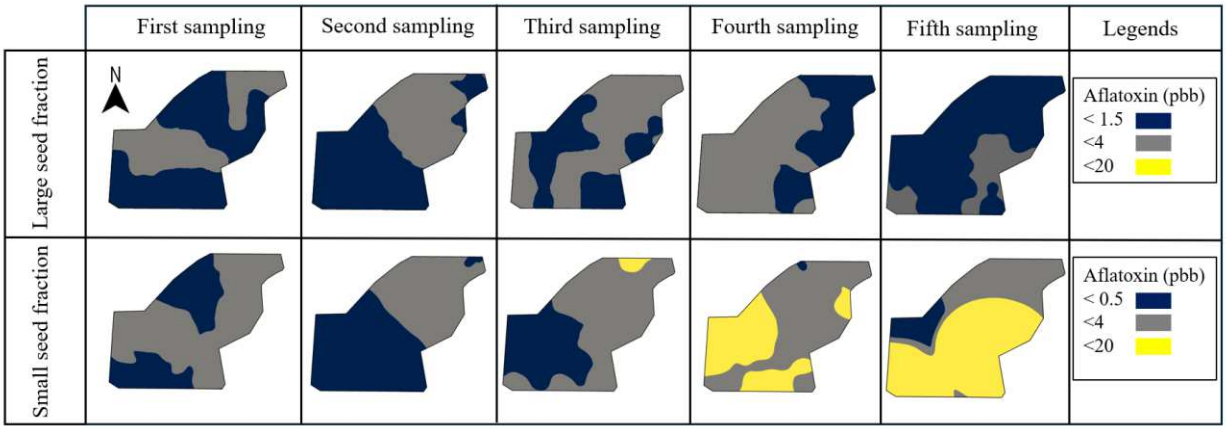


Figure 14. *Spatial distribution of aflatoxin concentration across five sampling events for small and large seed fractions Colors represent aflatoxin concentration categories (ppb).*

4. Discussion

4.1 Integration of Statistical Inference and Predictive Modeling

The combined analytical framework showed that statistical inference and predictive modeling provided complementary information about aflatoxin contamination. Inferential analyses demonstrated that differences between seed fractions varied across the growing season, while DAP-based trajectory analysis characterized these changes over time. Under nested cross-validation, direct contamination was more predictable than deviations from the expected seasonal trajectory, with stronger performance for the smaller fraction ($R^2 = 0.416$) than the larger fraction ($R^2 = 0.271$). The lower performance for deviations ($R^2 = 0.109–0.186$) indicates that much of the predictable variation was associated with broader seasonal progression, whereas anomalous variation was less well explained by the measured covariates.

4.2 Biological Interpretation of Seed-Fraction Differences

The temporal differences between seed fractions indicate that the relationship between seed size and aflatoxin contamination changed during crop development. Contamination was similar between fractions early in the season, diverged during the middle sampling periods, and converged again at the final sampling event, with the smaller fraction showing greater contamination during events 2-4. This pattern suggests that smaller seeds may become disproportionately represented among contaminated kernels during specific developmental or environmental conditions. However, seed fraction should be considered an associated phenotypic characteristic rather than a causal mechanism, as differences may reflect variation in kernel development, maturity, physiological stress, or damage.

The persistence of the mid-season seed-fraction divergence and the overall DAP-based trajectory difference under leave-one-field-out sensitivity analysis further indicates that these patterns reflected a multi-field response rather than being driven by a single field.

4.3 Episodic Contamination and Environmental Stress

Aflatoxin contamination showed an episodic rather than uniformly progressive pattern, with elevated concentrations occurring during specific sampling periods and at particular field locations. The spatial patterns further demonstrated localized variation that could be obscured by field-average measurements. Rainfall deficit, recent rainfall, and temperature repeatedly contributed to predictive performance, suggesting that contamination was associated with the timing and sequence of wet and dry conditions rather than with precipitation alone. The importance of 7- and 14-day weather variables further indicates that aflatoxin responses may integrate environmental conditions over multiple short-term time windows.

4.4 In-season Deviations as Indicators of Anomalous Risk

Modeling deviations from the expected seasonal trajectory provided a more stringent assessment of environmental associations because the general seasonal pattern had already been removed. Predictive performance declined substantially for these deviations, indicating that anomalous contamination was more difficult to explain than overall contamination. Nevertheless, recent rainfall, extended dry periods, and temperature variables remained among the leading predictors, with their relative importance differing between seed fractions. These results suggest that unmeasured biological and microscale environmental processes likely contribute substantially to unusually high or low contamination events.

4.5 Implications for Risk Management and Decision Support

The results indicate that both sampling strategy and environmental conditions are important for characterizing aflatoxin risk. Differences among sampling locations, sampling periods, and seed fractions suggest that a single field-average measurement may not fully represent within-field contamination risk. Short-term rainfall, dry-period, and temperature conditions during the one to two weeks preceding sampling also provided useful information about contamination status. However, the decline in performance under leave-one-field-out validation, including R^2 values of only 0.062 and 0.055 for direct contamination and negative R^2 values for deviation models, indicates that the models are not yet suitable as universally transferable forecasting tools.

4.6 Limitations and Future Research

The study was limited to five commercial fields and therefore represents a relatively narrow range of spatial and environmental conditions. Although nested cross-validation demonstrated useful predictive information within the observed field system, the reduced performance under leave-one-field-out validation highlights the need for broader field-level validation. Future studies should incorporate additional biological and microenvironmental measurements, along with more fields and growing seasons, to better explain extreme contamination events. Such data could improve model transferability and support the development of more robust aflatoxin risk-assessment tools.

Source of Funding

This research was supported by United States Peanut Federation and United States Department of Agriculture Research Service.

Conflicts of Interest

Conflicts of interest: None.

References

Adeyeye, S. A. O., & Adeyeye, B. R. (2026). Applications of artificial intelligence, internet of things and blockchain in prevention, control and detection of mycotoxins in cereals and legumes. *World Mycotoxin Journal*, *1*(aop), 1-36.

Aoun, M., Stafstrom, W., Priest, P., Fuchs, J., Windham, G. L., Williams, W. P., & Nelson, R. J. (2020). Low-cost grain sorting technologies to reduce mycotoxin contamination in maize and groundnut. Food Control, 118, 107363. https://doi.org/10.1016/j.foodcont.2020.107363

Bowen, K. L., & Hagan, A. K. (2015). Temperature and moisture conditions that affect aflatoxin contamination of peanuts. *Peanut Science*, *42*(2), 121-127.

Breiman, L. (2001). Random forests. *Machine Learning*, *45*(1), 5–32. https://doi.org/10.1023/A:1010933404324

Chen, T., & Guestrin, C. (2016). XGBoost: A scalable tree boosting system. In *Proceedings of the 22nd ACM SIGKDD International Conference on Knowledge Discovery and Data Mining* (pp. 785–794). Association for Computing Machinery. https://doi.org/10.1145/2939672.2939785

Cole, R. J., Sanders, T. H., Hill, R. A., & Blankenship, P. D. (1985). Mean geocarposphere temperatures that induce preharvest aflatoxin contamination of peanuts under drought stress. *Mycopathologia*, *91*(1), 41-46.

Colin Cameron, A., & Miller, D. L. (2015). A practitioner's guide to cluster-robust inference. *Journal of human resources*, *50*(2), 317-372.

Danso, J. K., Mbata, G. N., & Holton, R. L. (2024). Preharvest insect pests of peanuts and associated aflatoxin contaminants in Georgia, USA. Journal of Economic Entomology, 117(3), 993-1000.

Dorner, J. W., Cole, R. J., Sanders, T. H., & Blankenship, P. D. (1989). Interrelationship of kernel water activity, soil temperature, maturity, and phytoalexin production in preharvest aflatoxin contamination of drought-stressed peanuts. Mycopathologia, 105(2), 117–128. https://doi.org/10.1007/BF00444034

EU . 2010. "Commission Regulation (EC) no 165/2010 of 26 February 2010, Amending Regulation (EC) no 1881/2006 Setting Maximum Levels for Certain Contaminants in Foodstuffs as Regards Aflatoxins." Official Journal of the European Union 27, no. 2: 8–12.

Friedman, J. H. (2001). Greedy function approximation: A gradient boosting machine. *Annals of Statistics*, *29*(5), 1189–1232. https://doi.org/10.1214/aos/1013203451

Geurts, P., Ernst, D., & Wehenkel, L. (2006). Extremely randomized trees. *Machine Learning*, *63*(1), 3–42. https://doi.org/10.1007/s10994-006-6226-1

Hill, R. A., Blankenship, P. D., Cole, R. J., & Sanders, T. H. (1983). Effects of soil moisture and temperature on preharvest invasion of peanuts by the Aspergillus flavus group and subsequent aflatoxin development. *Applied and environmental microbiology*, *45*(2), 628-633.

Hoerl, A. E., & Kennard, R. W. (1970). Ridge regression: Biased estimation for nonorthogonal problems. *Technometrics*, *12*(1), 55–67. https://doi.org/10.1080/00401706.1970.10488634

Koshiol, J., Yadav, A., Groopman, J. D., & Dutta, U. (2026). Aflatoxins and Human Health: Global Exposure, Disease Burden, and One Health Strategies. Toxins, 18(2), 90. https://doi.org/10.3390/toxins18020090

Mshanga, J., Makule, E., & Ngure, F. (2023). Physical methods for reduction of aflatoxins exposure in groundnuts in some low-income countries: a review.

Perrone, G., Ferrara, M., Medina, A., Pascale, M., & Magan, N. (2020). Toxigenic Fungi and Mycotoxins in a Climate Change Scenario: Ecology, Genomics, Distribution, Prediction and Prevention of the Risk. Microorganisms, 8(10), 1496. https://doi.org/10.3390/microorganisms8101496

Whitaker, T. B., Dorner, J. W., Lamb, M., & Slate, A. B. (2005). The effect of sorting farmers' stock peanuts by size and color on partitioning aflatoxin into various shelled peanut grade sizes. *Peanut Science*, *32*(2), 103-118.